Journal of Applied Science and Technology (JAST), Vol. 20, Nos. 1 & 2, 2016, pp. 01 - 09

EFFECT OF PERMEABILITY ANISOTROPY ON FORCED CONVECTION THERMAL - HYDRODYNAMICS OF ENTRANCE AND DEVELOPED FLOW REGIMES IN POROUS SATURATED CIRCULAR TUBE

C. Akowanou, G. Degan and V. Prodjinonto
Laboratoire d'Energétique et de Mécanique Appliquées, Ecole Polytechnique d'Abomey-Calavi, Université d'Abomey-Calavi, Boite Postale 2009, Cotonou, Bénin

ABSTRACT

Forced convective flow through anisotropic porous saturated circular tube was analysed to determine the entrance length to the hydrodynamic flow. The porous medium saturated with an incompressible viscous fluid was characterized by anisotropy permeability ratio, inclination angle of the principal axes and Prandtl number. The flow field was a succession of two distinct flow regions, the entrance region followed by fully developed flow regime. The boundary-layer regime prevailing at the thermal entrance region was analysed by integral relations approach, and analytical expressions of the entrance length, wall friction and heat transfer rate were obtained. Limiting cases for flow applicable to low and high porosity media were also observed. The anisotropic properties of the porous medium were significant where permeability ratio was either greater or less than 1.

Keywords: Forced convection, Porous medium, Hydrodynamic flow field, Anisotropy Permeability ratio, Wall friction

1. INTRODUCTION

Flow through cylindrical channels filled with saturated porous media is of considerable importance in engineering applications, such as electronic cooling systems, solid matrix heat exchangers, geothermal system, underground gas drainage, petroleum extraction, storage of agriculture products, catalytic converters, etc. Analysis of thermal development length through a porous channel maintained at uniform temperature for both parallel-plate channel and circular tube has been reported [1]. Thermal energy equations for viscous dissipation and flow work on forced convection in a channel filled with saturated porous medium have been solved for both isothermal and iso-flux walls [2].

Equations for forced convection in a fluid saturated porous medium tube with isoflux wall have been solved analytically by asymptotic techniques [3, 4]. The problem of thermal boundary-layer along an isothermal cylinder in a porous medium has been solved numerically, and also by the method of extended perturbation series, where the thermal boundary-layer thickness increased with increase in the transverse curvature parameter of the cylinder [5].

In recent engineering applications, anisotropic porous media commonly used include fibrous materials, biological materials, geological formations and oil extraction. Anisotropy is a consequence of preferential orientation and asymmetric geometry of the grain or fibbers which constitute the porous medium. Despite the many applications, convection in anisotropic porous media has not been extensively researched.

The effect of anisotropy on convective stability of a porous layer has been conducted [6]. The onset of convection in anisotropic porous layer in which the principal axes were obliquely oriented to gravity vector has been studied, whereby new flow patterns with tilted plane of motion or tilted lateral cell walls were obtained [7]. Analytical study on forced convection in horizontal channel filled with anisotropic porous medium of permeability principal axes oriented in a direction oblique to gravity vector has shown that both the permeability ratio and inclination angle of the principal axes had strong influence on the convective heat transfer in the horizontal porous channel [8].

In this paper, the research conducted to examine the effects of anisotropic permeability and orientation angle on a porous matrix in the development of convective boundary-layer flow, hydrodynamic entrance length preceding a fully developed flow regime, and heat transfer through the porous circular tube are presented. Equations of the entrance length, wall friction and heat transfer rate were obtained, and limiting cases for flow applicable to low and high porosity media were also analysed. The anisotropic properties of the porous medium on the problem were significant where the permeability ratio was either greater or less than 1.

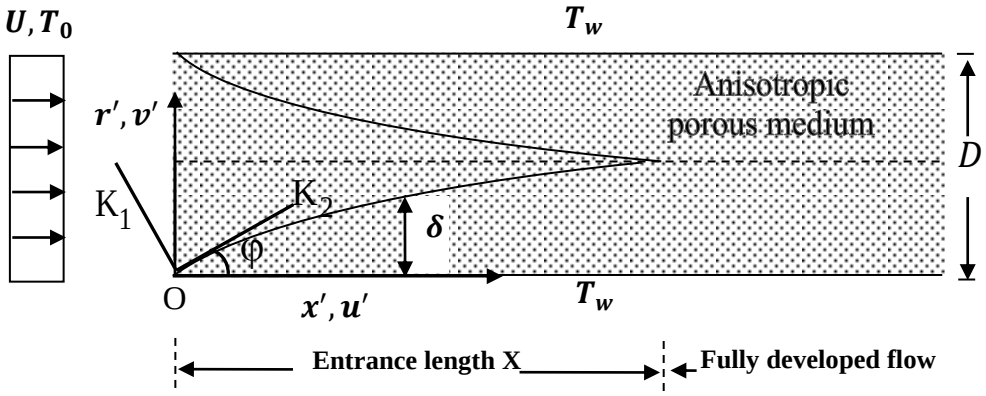

Fig. 1. Coordinate system for developing flow in the entrance region of the cylindrical porous tube

2. CONCEPTUAL MODEL

The physical domain consisted of a horizontal cylindrical channel filled with a porous medium of anisotropic permeability as shown in Fig. 1. The fluid entered the two dimensional channel at steady-state flow at uniform velocity U and temperature T_0. The anisotropy permeability of the porous medium was characterized by permeability ratio $K^* = K_1/K_2$, and inclination angle φ between the horizontal direction and principal axis with the permeability. K_1 and K_2 are permeability along the two principal axes. The rotation took place about the horizontal x' axis from which the anisotropic rotation angle φ was encountered.

The cylindrical coordinates (x', r') as system coordinate (x', r') were used as the framework for axisymmetric flow field. The horizontal cylinder was heated at uniform temperature T_w at the wall. The porous medium was saturatated with an incompressible viscous fluid, which was in local thermodynamic equilibrium with the solid matrix.

From the entrance of the channel, the flow field was a succession of two distinct flow regions. In the entrance region, the fluid motion was affected by the obstruction effect introduced by the solid wall. The boundary-layers expanded close to the channel's walls and coexisted with the core fluid that had not been influenced by the presence of the walls. The entrance length corresponded to the distance from the beginning of the tube to the position where the two boundary-layers merged. Beyond the first region, the core disappeared and the boundary layers were no longer distinct, but gave rise to a fully developed flow regime.

3. MATHEMATICAL FORMULATION

The equations governing conservation of mass, momentum and energy for steady forced convective flow in anisotropic porous medium with permeability anisotropy were [8],

$$\nabla.\overrightarrow{V'} = 0 \quad (1)$$

$$\overrightarrow{V'} = \frac{\overline{\overline{K}}}{\mu}\left(-\nabla p' + \mu_{eff}\nabla^2\overrightarrow{V'}\right) \quad (2)$$

$$\left(\rho c_p\right)_f \nabla.\left(\overrightarrow{V'}T'\right) = k\nabla^2 T' \quad (3)$$

where $\overrightarrow{V'}$ is superficial flow velocity, p' is pressure, μ is dynamic viscosity, ρ is density, μ_{eff} is apparent dynamic viscosity for Brinkman's model, $\left(\rho c_p\right)_f$ is heat capacity of the fluid, k is thermal conductivity and T' is temperature. The symmetrical second-order permeability tensor $\overline{\overline{K}}$ was expressed by [8],

$$\overline{\overline{\mathrm{K}}} = \begin{bmatrix} \mathrm{K_2}\cos^2\varphi + \mathrm{K_1}\sin^2\varphi & (\mathrm{K_2} - \mathrm{K_1})\sin\varphi\cos\varphi \\ (\mathrm{K_2} - \mathrm{K_1})\sin\varphi\cos\varphi & \mathrm{K_2}\sin^2\varphi + \mathrm{K_1}\cos^2\varphi \end{bmatrix} \quad (4)$$

In physical variables (r',u'), the governing eqns. (1) - (3) were rewritten as;

$$\frac{\partial}{\partial x'}(r'u') + \frac{\partial}{\partial r'}(r'v') = 0 \quad (5)$$

$$au' - cv' = \frac{K_1}{\mu}\left[-\frac{\partial p'}{\partial x'} + \mu_{eff}\left(\frac{\partial^2 u'}{\partial x'^2} + \frac{1}{r'}\frac{\partial u'}{\partial r'} + \frac{\partial^2 u'}{\partial r'^2}\right)\right] \quad (6)$$

$$-cu' + bv' = \frac{K_1}{\mu}\left[-\frac{\partial p'}{\partial r'} + \mu_{eff}\left(\frac{\partial^2 v'}{\partial x'^2} + \frac{1}{r'}\frac{\partial v'}{\partial r'} + \frac{\partial^2 v'}{\partial r'^2}\right)\right] \quad (7)$$

$$\left(\rho c_p\right)_f\left(u'\frac{\partial T'}{\partial x'} + v'\frac{\partial T'}{\partial r'}\right) = k\left(\frac{\partial^2 T'}{\partial x'^2} + \frac{1}{r'}\frac{\partial T'}{\partial r'} + \frac{\partial^2 T'}{\partial r'^2}\right) \quad (8)$$

where

$\mathrm{a} = \sin^2\varphi + \mathrm{K}^*\cos^2\varphi$, $\mathrm{b} = \cos^2\varphi + \mathrm{K}^*\sin^2\varphi$, and

$$\mathrm{c} = \frac{1}{2}(1 - \mathrm{K}^*)\sin 2\varphi \quad (9)$$

In the boundary-layer regime in which most of the fluid motion is restricted to a thin layer along the channel's walls, the velocity increased from the wall (where $u' = 0$) to the center of the channel (for which $u' = U_c$), so that the boundary-layer expanded in the x direction, at the neighborhood of each wall. Outside the boundary layer, a free stream in a flow region (the center region) occurred in the porous medium, not affected by the obstruction introduced by the solid wall and characterized by the velocity $u' = U_c$, $v' = 0$ with a pressure $p' = P_c$.

If order of magnitude of the distance in which u' changed from 0 to U_c was δ, and T' from T_w to T_c was δ_T, the boundary conditions associated with eqns. (5 - 8) were,

$$\begin{cases} r' = 0: & u' = 0 \\ r' = \delta: & u' = U_c, \ v' = 0 \end{cases} \quad (10a)$$

and

$$\begin{cases} r' = 0: & T' = T_w \\ r' = \delta_T: & T' = T_c \end{cases} \quad (10b)$$

where δ and δ_T are respectively the dynamic and thermal boundary-layer thickness and T_c is temperature in the core region where the free stream was uniform.

4. ANALYSIS OF ANALYTICAL SOLUIONS

4.1. Entrance length X

In the slender region ($\delta \times L$) such that $\delta \ll L$ identified the scales for x, r' and u' [9];

$$x' \sim L, \quad r' \sim \delta, \quad u' \sim U_c \quad (11)$$

The conservation eqns. (5) and (6) required the balances,

$$\frac{U_c}{L} \sim \frac{v'}{\delta} \quad (12)$$

$$\left(a\frac{U_c}{K_1}, \quad c\frac{v'}{K_1}\right) \sim \left(\frac{1}{\mu}\frac{P_c}{L}, \quad \frac{\mu_{eff}}{\mu}\frac{U_c}{L^2}, \quad \frac{\mu_{eff}}{\mu}\frac{U_c}{\delta^2}\right) \quad (13)$$

Solving the balance for δ,

$$\delta \sim LDa^{1/2}a^{-1/2} \quad (14)$$

Considering the slenderness of the boundary-layer region and making use of eqn. (11), $v' = 0$, the momentum eqn. (6) reduced to

$$a\frac{u'}{K_1} = -\frac{1}{\mu}\frac{\partial p'}{\partial x'} + \frac{\mu_{eff}}{\mu}\frac{\partial^2 u'}{\partial r'^2} \quad (15)$$

For the slenderness boundary layer region of interest ($\delta \times L$), $\partial p'/\partial x' = dP_c/dx'$ [9], and upon integration of eqn. (15) over the region in which $(\partial/\partial r')|_{r'=\delta} = 0$, yielded,

$$\frac{a}{K_1}\int_0^\delta u'\,dr' = -\frac{1}{\mu}\frac{dP_c}{dx'}\int_0^\delta dr'' - \frac{\mu_{eff}}{\mu}\left(\frac{\partial u'}{\partial r'}\right)_{r'=0} \quad (16)$$

The value of μ_{eff} was taken, as a first approximation, to be equal to μ (i.e, $\mu_{eff} \approx \mu$) [9].

Applying Bernoulli's equation in the core region, $\rho U_C^2/2 + P_C = constant$, the pressure gradient dP_C/dx' was deduced, and dividing eqn. (16) by U_C,

$$\frac{a}{K_1}\int_0^\delta \frac{u'}{U_c}dr' = \frac{\delta}{\gamma}\frac{dU_C}{dx'} - \frac{1}{U_c}\left(\frac{\partial u'}{\partial r'}\right)_{r'=0} \quad (17)$$

Applying the boundary conditions eqn. (10.a), the velocity profile shape was obtained as,

$$\frac{u'}{U_c} = \frac{1}{3}\left[8\left(\frac{r'}{\delta}\right) - 9\left(\frac{r'}{\delta}\right)^2 + 4\left(\frac{r'}{\delta}\right)^3\right] \quad (18)$$

The mass conservation in the half-width of the channel (from $r' = 0$ to $r' = D/2$) required

$$\int_0^\delta \rho u'\,dr' + \int_\delta^{D/2} \rho U_c\,dr' = \rho\, U\, \frac{D}{2} \quad (19)$$

Substituting eqn. (18) into eqn. (19) and dividing by U_C, and integrating, the boundary-layer thickness δ was expressed as,

$$\frac{\delta(x')}{D/2} = 3\left(1 - \frac{U}{U_c}\right) \quad (20)$$

Using eqn. (18), the integration of eqn. (17) yielded,

$$\frac{9}{4}\frac{D^2}{\gamma}\left(1 - \frac{U}{U_c}\right)^2 dU_c - \left[\frac{8}{3} + 6\frac{a}{Da}\left(1 - \frac{U}{U_c}\right)^2\right]dx' = 0 \quad (21)$$

Integrating eqn. (21) with the condition $\delta = 0$ at the channel's inlet ($x' = 0$) yielded,

$$\frac{32}{27}\left(\frac{x'/D}{Re_D}\right) = A\left(\frac{U_c}{U} - 1\right) - A^2\left\{ln\left(\frac{\left(\frac{U}{U_c}\right)^2}{1+\alpha\left(1-\frac{U}{U_c}\right)^2}\right) + \left(\frac{1-\alpha}{\sqrt{\alpha}}\right)Arctan\left(\left(1-\frac{U}{U_c}\right)\sqrt{\alpha}\right)\right\} \quad (22)$$

where

$$A = \frac{1}{1+\alpha}, \ \alpha = \frac{9}{4}\varsigma^2, \ \varsigma^2 = \frac{a}{Da} \quad (23)$$

$Da = K_1/R^2$ is the Darcy number, where R is channel radius.

Defining X as inlet location from the entrance, the entrance length where the two boundary-layers merged, $\delta(X) = D/2$, and eqn. (20) showed that $U = (2/3)U_C$. Hence, from eqn. (22), the entrance length was expressed as,

$$\frac{X/D}{Re_D} = \frac{27}{32}\left\{\frac{A}{2} + A^2\left[ln\left(\frac{4}{9+\alpha}\right) + \left(\frac{1-\alpha}{\sqrt{\alpha}}\right)arctan\left(\frac{\sqrt{\alpha}}{3}\right)\right]\right\} \quad (24)$$

where $\alpha = (9\varsigma^2)/4$. From eqn. (24), the two cases of interest were $\varsigma \ll 1$ for high porosity media and $\varsigma \gg 1$ for low porosity media.

High porosity media, $\varsigma \ll 1$, corresponded to a weaker anisotropic porous medium ($a \ll Da$) for which the resistance due to the

boundary effects was not dominant as compared to that of the solid matrix ($Da \to \infty$). The situation approached to the fluid medium, where anisotropic effects were not significant. In the limit $\to \infty$ ($\varsigma \to 0$); eqn. (24) for the entrance length became,

$$\frac{X/D}{Re_D} = \frac{27}{32}\left\{\frac{1-\alpha}{2} + (1-2\alpha)\left[ln\frac{4}{9} + \frac{9-10\alpha+\alpha^2}{27}\right]\right\} \quad (25)$$

and as $\alpha \to 0$, the entrance length reached the limiting value,

$$\lim_{\alpha\to 0}\left(\frac{X/D}{Re_D}\right) = \frac{27}{32}\left(\frac{5}{6} + 2\ ln\frac{2}{3}\right) = 0.019 \quad (26)$$

Low porosity media with $\varsigma \gg 1$, corresponded to pure Darcy medium ($Da \ll a$) for which the anisotropic effects were dominant, as $Da \to 0$ and $\varsigma \to \infty$. Hence, the entrance length through the channel was calculated from

$$\frac{X/D}{Re_D} \approx \frac{27}{64(1+\alpha)} \quad (27)$$

and as $\varsigma \to \infty$, in the limit $\alpha \to \infty$, the entrance length through the channel reduced to $(X/D)/Re_D \to 0$.

4.2. Wall friction

The wall friction defined as [9],

$$C_{f,x'} = \frac{\mu\frac{\partial u\prime}{\partial r\prime}\Big|_{r'=0}}{\frac{1}{2}\rho U^2} \quad (28)$$

was deduced from velocity profile eqn. (18) as,

$$C_{f,x'}Re_D = \frac{32}{9}\left\{\frac{U}{U_C}\left(1-\frac{U}{U_C}\right)\right\}^{-1} \quad (29)$$

At location X, a measured distance from the channel's entrance to the position where the two boundary layers merged, $U/U_C = 2/3$, and the limiting value of the wall friction became,

$$C_{f,x'}Re_D = 16 \quad (30)$$

4.3. Heat transfer rate

For the heating effect on channel's wall in the thermal boundary-layer region ($\delta_T \times L$), of thickness $r' \sim \delta_T$ and length $x' \sim L$, the conservation of energy eqn. (8) required the balance,

$$\left(\frac{U_c\Delta T}{L},\ \frac{v\prime\Delta T}{\delta_T}\right) \sim \left(\frac{\alpha\Delta T}{L^2},\ \frac{\alpha\Delta T}{\delta_T^2}\right) \quad (31)$$

where $\Delta T = (T_w - T_c)$ is characteristic scale of temperature, T_c is temperature in the core region where the free stream was uniform.

Solving the balance for the thermal boundary layer thickness δ_T,

$$\delta_T \sim LRe_L^{-1/2}Pr^{-1/2} \quad) \quad (32)$$

Applying $\delta_T \ll L$, order-of-magnitude, eqn. (8) reduced to

$$\frac{\partial(u\prime T\prime)}{\partial x\prime} + \frac{\partial(v\prime T\prime)}{\partial r\prime} + \frac{v\prime T\prime}{r\prime} = \alpha\left(\frac{\partial^2 T\prime}{\partial r\prime^2}\right) \quad (33)$$

Over the region ($\delta_T \times L$), the free stream was uniform, and consequently $(\partial/\partial r')|_{r'=\delta_T=0}$, $T = T_c$, and upon integration of eqn. (33) from $r' = 0$ to $r' = \delta$,

$$\frac{d}{dx}\left(\int_0^{\delta_T} u'T'dr'\right) + v'_{\delta_T}T'_c - v'_0T'_c = -\alpha\left(\frac{\partial T_L}{\partial r\prime}\right)_{r\prime=0} \quad (34)$$

Since the wall was impermeable, $v'_0 = 0$ and v'_{δ_T} was evaluated by integrating the continuity eqn. (5) from $r' = 0$ to $r' = \delta_T$ to give,

$$v'_{\delta_T} = -\frac{d}{dx\prime}\int_0^{\delta_T} u'\,dr' \quad (35)$$

Substituting v'_{δ_T} into eqn. (34) into eqn. (35),

$$\frac{d}{dx'}\int_0^{\delta_T} u'\,(T_c - T')dr' = \alpha\left(\frac{\partial T_L}{\partial r'}\right)_{r'=0} \quad (36)$$

Applying boundary conditions eqn. (10.b), the temperature profile shape equation became,

$$T' - T_c = \Delta T\left(1-\frac{r\prime}{\delta_T}\right)^2 \quad (37)$$

Substituting eqns. (18) and (37) into eqn. (36), and integrating,

$$\frac{\Delta^3}{3}\left(\frac{\Delta^2}{15} + \frac{3\Delta}{10} - \frac{2}{3}\right) = \frac{3}{4}\ \frac{1}{Pr}\ \frac{1-\frac{U}{U_c}}{\left[1+\alpha\left(1-\frac{U}{U_c}\right)^2\right]} \quad (38)$$

where $\Delta\ (= \delta_T/\delta)$ is relative size of thermal and dynamic boundary-layers. From the entrance of the channel to the location X where the two boundary layers merged, the dynamic boundary layer thickness δ increased from zero to $D/2$ $(i.e.,\ 0 \ll \delta \ll D/2)$, and by eqn. (20), $2/3 \ll U/U_c \ll 1$.

The local Nusselt number Nu, in the thermal developing region was defined as the heat transfer over the pure heat conduction through the channel,

$$Nu = \frac{hD}{k} \quad (39)$$

where $h = q/(T_w - T_c)$ is local heat transfer coefficient and $q = -k(\partial T'/\partial r')|_{r'=0}$ is local surface heat flux in the heated channel. From eqns. (20), (38) and (39), the expression for Nusselt number became,

$$Nu = \frac{4}{3\Delta}\left(1-\frac{U}{U_C}\right)^{-1} \quad (40)$$

From eqns. (14) and (32), the relative size of thermal and dynamic boundary layers Δ had the scale,

$$\Delta \sim \frac{a^{1/2}}{Da^{1/2}Pr^{1/2}Re_L^{1/2}} \quad (41)$$

The boundary-layer was analysed for the two cases of interest, $\Delta \ll 1$ and $\Delta \gg 1$.

Table 1. Values of $(X/D)/Re_D$ by different method

$(X/D)/Re_D$		
Similarity solution	**Integral relations approach**	
Blasius's solution [14]	Bejans' solution [14]	Present study eqn.(26)
0.01	0.026	0.019

For $\Delta \ll 1$, applicable to the saturating fluids, such as water or oils; the condition was equivalent to $\delta \gg \delta_T$, and therefore valid strictly in the limit of Prandtl number Pr,

$$Pr \ll \frac{a}{Re_L Da} \quad (42)$$

For $\Delta \gg 1$, applicable to liquid metals saturating the porous medium, the equivalent condition $\delta \ll \delta_T$, was therefore valid strictly in the limit,

$$Pr \gg \frac{a}{Re_L Da} \quad (43)$$

From eqn. (38), Δ depended on the anisotropic parameters $K^*$and φ of the porous medium, as observed for Nu in eqn. (40).

4.4. Numerical Calculations and Plots of Solutions

Using $Pr = 500$, corresponding to saturating fluid of water or oil, values of K^*, φ $(a = sin^2\varphi + K^* cos^2\varphi)$, and Darcy number Da, the values of Δ were calculated from eqn. (38), with the condition that $2/3 \ll U/U_c \ll 1$; and used to calculate parameters δ, $C_{f,x'}$, Nu and $(X/D)/Re_D$, for the solutions to be plotted.

5. RESULTS

5.1. Data validation

The integral relations approach used to study the problem of boundary-layer regime was validated by comparing calculated value of $(X/D)/Re_D$ in Table 1, with published data obtained using a similarity solution and integral approach [14]. By estimating X and assuming $\delta(X) = D/2$, the extent of the laminar developping region X scaled with DRe_D and the proportionality factor was of order 10^{-2} [14].

From eqns. (18) and (28), the wall friction was deduced at location X where $U/U_C = 2/3$, the limit value of $C_{f,x'}Re_D = 16$ (eqn.(30)), in agreement with the published data using the integral approach to solve the problem of hydrodynamic entrance length for laminar flow duct [14].

5.2. Effect of Boundary layer thickness

The boundary layer thickness $\delta/(D/2)$ was plotted in Fig. 2(a) as a function of entrance length for values of anisotropic permeability ratio K^* (0.01, 0.50, 1.0 and 2.0) and $\varphi = 45°$. The boundary-layer thickness decreased with respect to that of an isotropic porous medium corresponding to $K^* = 1$, when the $K^* < 1$.

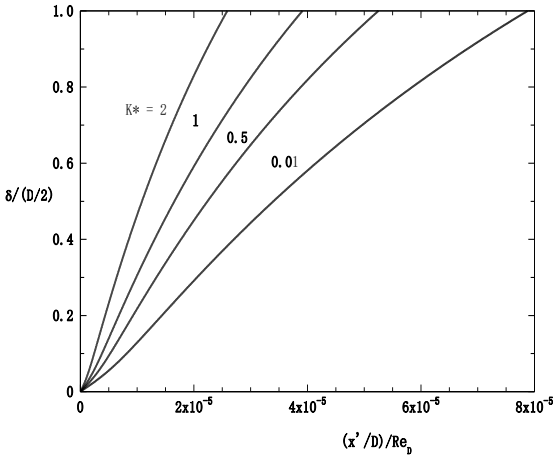

Fig. 2(a). Variation of boundary-layer thickness $\delta/(D/2)$ against entrance length $(x'/D)/Re_D$ for $Da = 10^{-4}$, $\varphi = 45°$ and different K^* values

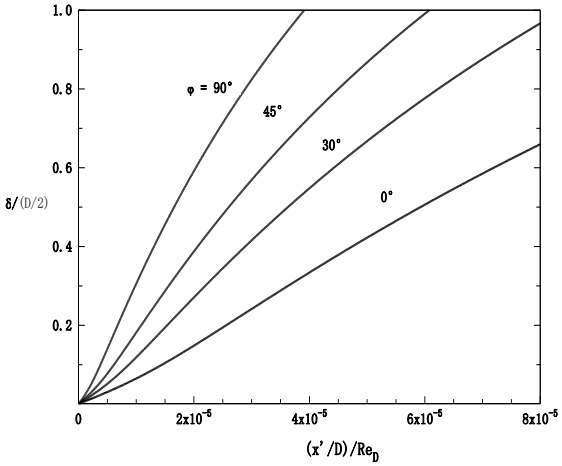

Fig. 2(b). Variation of boundary-layer thickness $\delta/(D/2)$ against entrance length $(x'/D)/Re_D$ for $Da = 10^{-4}$, $K^* = 0.3$ and different φ values

Fig. 2(b) illustrates the influence of incclination φ of the principal axes of the porous medium on the boundary layer thickness when $K^* = 3 \times 10^{-1}$ and $Da = 10^{-4}$. The boundary layer thickness increased with increase of inclination of the principal axes. For $Da < 1$, i.e.,

K_1 value of $K^* < 1$ when $\varphi = 0°$, the situation corresponded to an increase of permeability K_2 in the horizontal direction promoting the forced circulation within the channel.

5.3. Effect of Wall friction

The wall friction $C_{fx'}Re_D$, was plotted in Fig. 3(a) as a function of the entrance length $(x'/D)/Re_D$ for different values of φ of the principal axes of the porous medium when $Da = 10^{-4}$ and $K^* = 3 \times 10^{-1}$. In the neighborhood of the entrance, the wall friction depended strongly on the anisotropic parameters K^* and φ. For a given entrance length, the wall friction decreased when the inclination φ of the principal axes was increased.

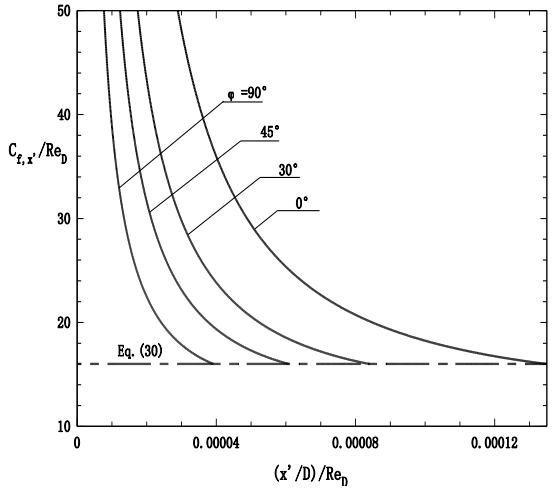

Fig. 3(a). Variation of wall friction $C_{fx'}Re_D$ against entrance length $(x'/D)/Re_D$ for $Da = 10^{-4}$, $K^* = 0.3$ and different φ values

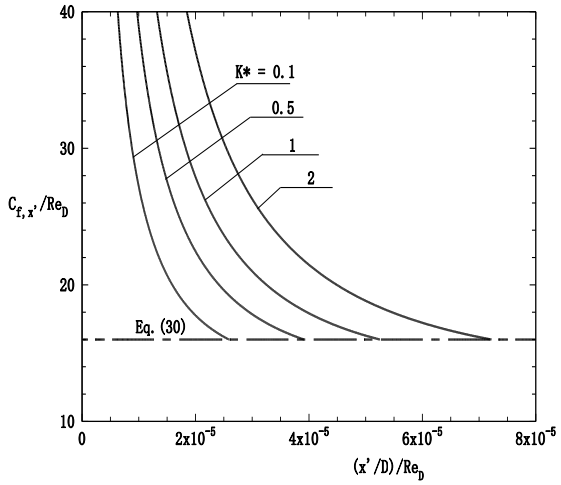

Fig. 3(b). Variation of wall friction $C_{fx'}Re_D$ against entrance length $(x'/D)/Re_D$ for $Da = 10^{-4}$, $\varphi = 45°$ and different K^* values

Figure 3(b) shows plot of wall friction $C_{fx'}Re_D$, as a function of the entrance length $((x'/D)/Re_D)$ for values of K^* of the porous medium when $Da = 10^{-4}$and $\varphi = 45°$. The wall friction was enhanced when $K^* < 1$ (i.e., $K^* = 0.1$) and weakened when $K^* > 1$ (i.e., $K^* = 10$), in comparison with that of an isotropic porous medium for which $K^* = 1$.

5.4. Effect of Entrance length

Fig. 4(a) illustrates the entrance length $(x'/D)/Re_D$ as a function of Darcy number Da for values of K^* when $\varphi = 45°$. In pure Darcy medium ($Da \to 0$), the entrance length increased as $K^*$was made smaller. The location where the two boundary-layers merged was pre-dicted as $(x'/D)/Re_D) \to 0$ when Da was small enough ($Da \to 0$).

The effect of varying the inclination φ of the principal axes of permeability on the entrance length $(x'/D)/Re_D$ was plotted in Fig. 4(b) as a function of Da when $K^* = 0.1$. The entrance length decreased as the inclination angle was increased from zero towards 90°

5.5. Effect of Nusselt number

Figure 5 shows the effects of varying the anisotropic angle φ on the Nusselt number in the entrance region when $Da = 10^{-4}$, $K^* = 3$ for $Pr = 500$ (saturating fluids). The heat transfer decreased rapidly at the entrance of the tube when the fluid flow through the porous medium.

Figure 5(b) shows the influence of K^* on Nu in the entrance region for $Da = 10^{-4}$ and $\varphi = 45°$ for the saturating fluids as water and oils ($Pr = 500$).

6. DISCUSSION

For a given location $(x'/D)/Re_D$ of the entrance of the channel, as $K^* > 1$, the boundary layer thickness increased rapidly and reached the limit $(D/2)$ at the centerline.

The fluid friction was reduced through the porous matrix and on the bounding wall so that the boundary-layer's thickness decreased. Therefore, the boundary-layer thickness was maximum at $\varphi = 90°$, i.e., when the permeability in the vertical direction was maximum, but minimum at $\varphi = 0°$, i.e., when the permeability in the vertical direction was minimum. From the results, the boundary-layer expanded and

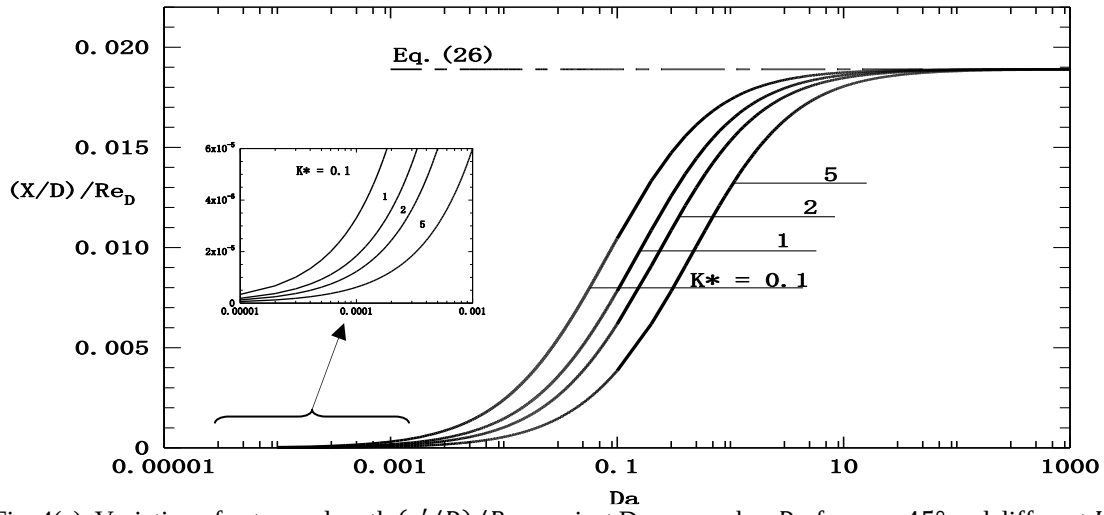

Fig. 4(a). Variation of entrance length $(x'/D)/Re_D$ against Darcy number Da for $\varphi = 45°$ and different K^* values

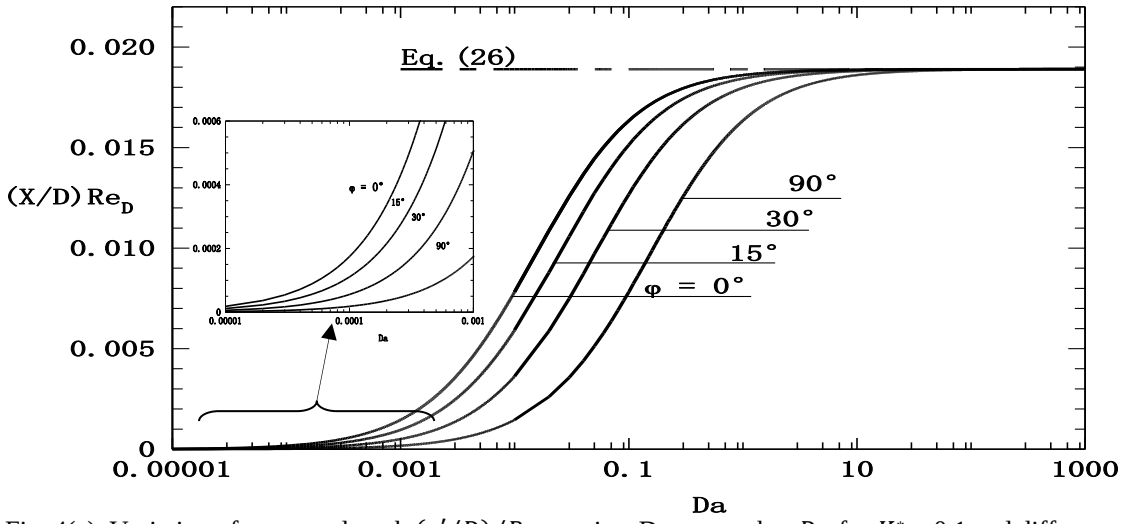

Fig. 4(a). Variation of entrance length $(x'/D)/Re_D$ against Darcy number Da for K^* = 0.1 and different φ values

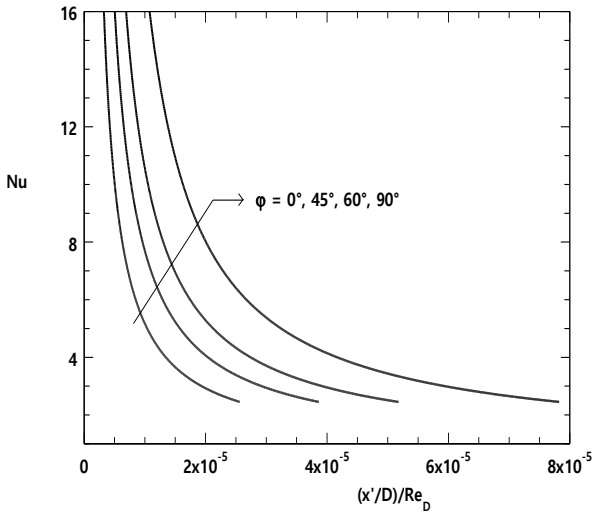

Fig. 5(a). Variation of Nusselt number (Nu) against entrance length $(x'/D)/Re_D$ in the boundary-layer region for the saturating fluid (water and oil, $Pr = 500$) for $Da = 10^{-4}$, $K^* = 3$ and different various values of φ

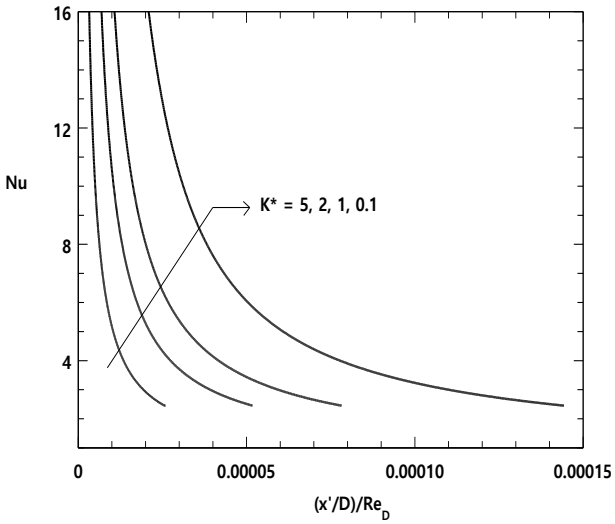

Fig. 5(b). Variation of Nusselt number (Nu) against entrance length $(x'/D)/Re_D$ in the boundary-layer region for the saturating fluid (water and oil, $Pr = 500$) for $Da = 10^{-4}$, $\varphi = 45°$ and different various values of K^*

reduced the entrance length preceding the fully developed flow when the principal axis with higher permeability was parallel to gravity.

As the fluid flow in the porous channel, the wall friction decreased abruptly and reached the minimum value, independent of φ, and corresponding to that obtained at the position where the two boundary-layers merged. The entrance length at the minimum value of wall friction increased when the anisotropic orientation φ was made weaker.

The observed behavior could be explained that for a given value of Da (i.e., K_1), an increase (a decrease) in K^* corresponded to a decrease (increase) of the permeability K_2, i.e., to a weaker (stronger) forced flow. Therefore, when the permeability of the porous was increased, the bulk frictional drag induced by the solid matrix to slow the fluid motion became gradually less and less important and reduced to the boundary frictional resistance.

In the pure Darcy medium, the bulk frictional drag induced by the solid matrix to slow the fluid motion reduced strongly the entrance length and favored the flow to be fully developed in the neighborhood of the tube's entrance. When Da was high enough, i.e., the resistance resulting from the boundary effects was dominant compared to the resistance from the solid matrix, the entrance length approached that for pure viscous fluid, $(x'/D)/Re_D \approx 0.02$), which was independent of anisotropy of the porous medium.

The maximum value of entrance length obtained was $(x'/D)/Re_D \approx 0.02$ when $\varphi = 0°$, was due to the fact that, when $K^* < 1$, the axis with higher permeability (K_2) was oriented in a direction which optimized the flow motion intensity.

The convective heat transfer was maximum at $\varphi = 90°$, i.e., when the permeability in the horizontal direction was maximum, but minimum at $\varphi = 0°$, i.e., when the permeability in the horizontal direction was minimum. For a given location in the entrance region of the tube, the convective heat transfer was enhanced when $K^* < 1$ and weakened when $K^* > 1$ in comparison with that of an isotropic medium, $K^* = 1$.

7. CONCLUSIONS

Forced thermal convection flow within a porous tube was controlled by anisotropic permeability ratio K^*, inclination angle φ of the principal axes of the medium and Prandtl number Pr.

In pure Darcy medium $Da \to 0$, the bulk frictional drag induced by the solid matrix to slow the fluid motion reduced considerably the entrance length and favoured the flow to be fully developed in the neighborhood of the entrance to the tube. The entrance length was enhanced where $K^* < 1$ and weakened where $K^* > 1$ in comparison with that of isotropic porous medium ($K^* = 1$). In the fluid medium $Da \to \infty$, the resistance from the boundary effects was dominant, the entrance length approached that for pure viscous fluid and became independent of the anisotropy of the porous medium.

The dynamic boundary-layer expanded quickly and reduced the entrance length preceeding the fully developed flow when the orientation of the principal axis with higher permeability of the anisotropic porous channel reaches the vertical direction.

In the entrance region, the heat transfer rate in the boundary-layer region was maximum when the porous matrix was oriented in direction that the principal axis with higher permeability was parallel to the flow direction, but minimum if perpendicular to the flow direction.

8. REFERENCES

1. Nield D.A., Kuznetsov A.V. and Xiong M., Thermally developing forced convection in a porous medium: parallel-plate channel or circular tube with isothermal walls, *J. Porous Media*, Vol. 7, 1985, pp. 19–27
2. Hooman K.H. and Gurgenci H., Effects of viscous dissipation and boundary conditions on forced convection in a channel occupied by a saturated porous medium, *Trans. Porous Media*, Vol. 68, 2007, pp. 301-309
3. Hooman K. and Ranjbar-Kani A., Forced convection in a fluid-saturated porous medium tube with isoflux wall, *Int. Commun Heat Mass Transf.*, Vol. 30, 2003, pp. 1015-1026
4. Hooman K. and Ranjbar-Kani A., A perturbation based analysis to investigate forced convection in a porous saturated tube, *J. Comp. Appl. Math.*, Vol. 162, 2004, pp. 411-419
5. Vasantha R. and Nath G., Forced convection along a longitudinal cylinder embedded in saturated porous layer. *Int. J. Heat Mass Transf.*, Vol. 14, 1987, pp. 639-646.
6. McKibbin R., Thermal convection in a porous layer, effects of anisotropy and surface boundary

conditions. *Trans. Porous Media*, Vol. 1, 1984, pp. 271-292.
7. Tyvan P.A. and Storesletten L., Onset of convection in an anisotropic porous medium with oblique principal axes, *J. Heat Trans.f Jpn. Res.*, Vol. 14, 1991, pp. 609-24.
8. Degan G., Zohoun S. and Vasseur P., Forced convection in horizontal porous channels with hydrodynamic anisotropy, *Int. J. Heat Mass transfer*, Vol. 45, 2002, pp. 3181-3188
9. Bejan A. *Convection Heat Transfer*, 1984, John Wiley & Sons, New York.

Journal of Applied Science & Technology
ISSN 0855-2215, Vol. 20, Nos. 1 & 2, 2015

APPENDIX

I. Balance of δ determination (eqn. 14)

Following Bejan [9], in the slender region $\delta \times L$ such that $\ll L$, identify the following scales for x, r' and u' as $x' \sim L, \quad r' \sim \delta, \quad u' \sim U_c$. Then the conservation eqn. (5) and (6) require the following balances:

$$\frac{U_c}{L} \sim \frac{v'}{\delta} \tag{12}$$

$$\left(a\frac{U_c}{K_1}, \quad c\frac{v'}{K_1} \right) \sim \left(\frac{1}{\mu}\frac{P_c}{L}, \quad \frac{\mu_{eff}}{\mu}\frac{U_c}{L^2}, \quad \frac{\mu_{eff}}{\mu}\frac{U_c}{\delta^2} \right) \tag{13}$$

From eqn. 13, solving the balance for δ,

$$a\frac{U_c}{K_1} \sim \frac{\mu_{eff}}{\mu}\frac{U_c}{\delta^2}; \Longrightarrow \delta^2 \sim \frac{\mu_{eff}}{\mu}\frac{K_1}{U_c}\frac{U_c}{a}, \sim \frac{\mu_{eff}}{\mu}\frac{K_1}{a}$$

The value of μ_{eff} in Brinkman's extension [8] was taken, as a first approximation, to be equal to μ (i.e, $\mu_{eff} \approx \mu$). The balance for δ is written as $\delta^2 \sim \frac{K_1}{a}$

$$\Longrightarrow \frac{\delta^2}{L^2} \sim \underbrace{\left(\frac{K_1}{L^2}\right)}_{Da}\frac{1}{a} \Longrightarrow \delta \sim L\frac{Da^{1/2}}{a^{1/2}} \tag{14}$$

where Da is Darcy number.

II. Integration of eqn.14 to obtain eqn.16

Due to the slenderness of the boundary layer region of interest $(\delta \times L)$, $\partial p'/\partial x' = dP_c/dx'$ and the integration of eqn. (15) over this region in which $(\partial/\partial r')|_{r'=\delta} = 0$ yields

$$\frac{a}{K_1}\int_0^\delta u'\,dr' = -\frac{1}{\mu}\frac{dP_c}{dx'}\int_0^\delta dr' + \frac{\mu_{eff}}{\mu}\int_0^\delta \left(\frac{\partial^2 u'}{\partial r'^2}\right)dr' =$$

$$-\frac{1}{\mu}\frac{dP_c}{dx'}\int_0^\delta dr' + \frac{\mu_{eff}}{\mu}\int_0^\delta \frac{\partial}{\partial r'}\left(\frac{\partial u'}{\partial r'}\right)dr' = -\frac{1}{\mu}\frac{dP_c}{dx'}\int_0^\delta dr' +$$

$$\frac{\mu_{eff}}{\mu}\left[\underbrace{\left(\frac{\partial u'}{\partial r'}\right)_{r'=\delta}}_{0} - \left(\frac{\partial u'}{\partial r'}\right)_{r'=0}\right];$$

$$\frac{a}{K_1}\int_0^\delta u'\,dr' = -\frac{1}{\mu}\frac{dP_c}{dx'}\int_0^\delta dr'' - \frac{\mu_{eff}}{\mu}\left(\frac{\partial u'}{\partial r'}\right)_{r'=0} \tag{16}$$

III. Integration of eqn.17 using eqn.18 in order to obtain eqn. 21

$$\frac{a}{K_1}\int_0^\delta u'\,dr' = -\frac{1}{\mu}\frac{dP_c}{dx'}\int_0^\delta dr'' - \frac{\mu_{eff}}{\mu}\left(\frac{\partial u'}{\partial r'}\right)_{r'=0} \tag{16}$$

The value of μ_{eff} in Brinkman's extension [8] was taken, as a first approximation, to be equal to μ (i.e, $\mu_{eff} \approx \mu$). From Bernoulli's equation in the core region, $\rho U_C^2/2 + P_C = constant$, the pressure gradient dP_C/dx' was deduced, and by dividing eqn. (16) by U_C,

$$\frac{a}{K_1}\int_0^\delta \frac{u'}{U_c}dr' = \frac{\delta}{\gamma}\frac{dU_C}{dx'} - \frac{1}{U_c}\left(\frac{\partial u'}{\partial r'}\right)_{r'=0} \tag{17}$$

Using the velocity profile eqn. (18), $\frac{u'}{U_c} = \frac{1}{3}\left[8\left(\frac{r'}{\delta}\right) - 9\left(\frac{r'}{\delta}\right)^2 + 4\left(\frac{r'}{\delta}\right)^3\right]$, and calculations of eqn.(17) gives $\frac{a}{K_1}\left(\frac{2}{3}\delta\right) = \frac{\delta}{\gamma}\frac{dU_C}{dx'} - \frac{1}{U_c}\left(\frac{8}{3}\frac{U_C}{\delta}\right)$,

$$\Longrightarrow \quad \frac{\delta^2}{\gamma}\frac{dU_C}{dx'} = \frac{8}{3} + \frac{2}{3}\frac{a}{K_1}\delta^2$$

Making use of the boundary-layer thickness $\delta(x') = (3D/2)\left(1 - (U/U_c)\right)$,

$$\frac{9}{4}\frac{D^2}{\gamma}\left(1 - \frac{U}{U_c}\right)^2 dU_c - \left[\frac{8}{3} + 6\frac{a}{Da}\left(1 - \frac{U}{U_c}\right)^2\right]dx' = 0 \tag{21}$$

In eqn. (21), $Da\ (= K_1/R^2)$ is the Darcy number based on the radius R of the tube.

Nomenclature

a, b, c constants, eqn. (9)
C_p: specific heat of fluid at constant pressure, $JKg^{-1}K^{-1}$
$\vec{g}$ gravitational acceleration, m/s^2
k thermal conductivity of the fluid, $Wm^{-1}K^{-1}$
$\overline{\overline{K}}$ flow permeability tensor, eqn. (4)
K_1, K_2 flow permeability along the principal axes, m^2
K^* anisotropic permeability ratio, K_1/K_2
Da Darcy number, K_1/R^2
p' pressure, Pa
$\vec{V}'$ seepage velocity
u', v' velocity components, ms^{-1}
(x', r') cylindrical coordinate system
Nu Local Nusselt number, hD/k
Pe Péclet number, $(\rho c_p)_f RU/k$
Pr Prandtl number, ν/α
R channel radius, m
Re_D Reynolds number, UD/ν
Re_L Reynolds number, UL/ν
T Dimensionless temperature profile in the fully developed region
T_0 Inlet temperature, K
T_W Wall temperature, K
U_C Core velocity, ms^{-1}
ς parameter, eqn. (23)
δ dynamic boundary-layer thickness, m
δ_T thermal boundary-layer thickness, m
Δ relative size of thermal and dynamic boundary-layers thicknesses, δ/δ_T
ΔT characteristic scale of temperature, K
μ dynamic viscosity of the fluid, $kgm^{-1}s^{-1}$
μ_{eff} effective viscosity in the Brinkman term
ν Kinematic viscosity of the fluid, μ/ρ
φ inclination angle of principal axes
ρ density of the fluid, kgm^{-3}
(ρc_p) heat capacity of the fluid, $Jm^{-3}K^{-1}$
$'$ dimensional quantities
c refers to the core
o refers to inlet flow characteristics
w refers to wall